Common Microcirculatory Framework for Monitoring Integrated Microcirculation

Yuan Li
Chinese Academy of Medical Sciences & Peking Union Medical College
Bing Wang
Chinese Academy of Medical Sciences & Peking Union Medical College
Bingwei Li
Chinese Academy of Medical Sciences & Peking Union Medical College
Xiaoyan Zhang
Chinese Academy of Medical Sciences & Peking Union Medical College
Xueting Liu
Chinese Academy of Medical Sciences & Peking Union Medical College
Qin Wang
Chinese Academy of Medical Sciences & Peking Union Medical College
Mingming Liu (mingmingliu@imc.pumc.edu.cn)
Chinese Academy of Medical Sciences & Peking Union Medical College
Jian Zhang
Chinese Academy of Medical Sciences & Peking Union Medical College
Honggang Zhang
Chinese Academy of Medical Sciences & Peking Union Medical College
Ruijuan Xiu
Chinese Academy of Medical Sciences & Peking Union Medical College

Research Article

Keywords: normalization, microcirculation, common framework, microhemodynamics, microcirculatory oxygen

Posted Date: March 31st, 2021

DOI: https://doi.org/10.21203/rs.3.rs-374822/v1

Abstract

Wide variation in magnitudes, units, and ranges of the microcirculatory variables brings hindrance in describing and evaluating the integrated microcirculatory function of tissues. We designed to establish common microcirculatory framework that contains microhemodynamic and microcirculatory oxygen parameters. To integrate microcirculatory information, demo microcirculatory permutations were generated by a computer algorithm based on microcirculatory characteristics. Four dimensionless methods (Z-score, Min-max, L2, and median scaling) were applied to transform microcirculatory data set into the dimensionless form. Three-dimensional (3-D) common microcirculatory framework was constructed and visualized by using Python and Apache ECharts. The performance of the four dimensionless methods in the pre-processing of multiple microcirculatory variables and the establishment of the common microcirculatory framework were compared. Microhemodynamic and microcirculatory oxygen parameters were embedded in the common microcirculatory framework. After processing by Min-max normalization, the transformed multiple microcirculatory values remained positive with fixed range mapping within [0, 1] and maintained the identity property of microcirculation both of microhemodynamic and microcirculatory oxygen variables in the common microcirculatory framework. Conclusively, Min-max normalization displays preferable integration efficiency, compatibility, and adaptability in the establishment of the 3-D visualized multiparametric common microcirculatory framework.

Introduction

Microcirculation, consisting of arterioles, capillaries, and venules less than 150 μm in diameter, is a dynamic determinant contributing to the processes involved in the maintenance of metabolic homeostasis and exchange of material and bio-information, which is responsive to physiological and pathological condition[1,2]. The microvasculature exhibits characteristic phenotype, which has reached a consensus that functionally and structurally disturbed microcirculation has been identified to precede involvement in the pathogenesis and development of diseases [3–5]. Moreover, complexity [6,7] and integrity [8–10] are fundamental properties of microcirculation. Nevertheless, despite its significance in health and diseases, assessment of integrated microvasculature function became increasingly neglected in clinical condition during the last decades due to lack of proper methods.

The characteristics of multiple microcirculatory variables are highly varying in magnitudes, units, and ranges. Although various microcirculation function indicators were reported in previous studies, the analysis and interpretation of experimental results are mostly based on one single functional variable, which is a lack of integration and accuracy. Therefore, it possesses necessity and significance in establishing a common microcirculatory framework of organs and tissues and optimizing multiple parameters interpretation and visualization, which may contribute to the description and evaluation of microcirculatory function globally [11,12]. Generally, the common microcirculatory framework should include microcirculatory oxygen and microhemodynamic profiles. To date, multiple microcirculatory data

set remain inherently biased as a result of reasons ranging from organs and tissues handling to differences caused by the laser Doppler instrumentation. Furthermore, when comparing multiple microcirculatory variables, the differences in units and value ranges demand a proper normalization method, which can embed multiple microcirculatory variables into an integrated common framework for visualization and downstream analysis.

Dimensionless processing refers to the removal of mathematical units of data set with different dimensions through mathematical algorithms for the overall analysis, including normalization, standardization, and scaling algorithm [13–15]. Moreover, to avoid that the analytic results of microcirculation varying greatly due to multiple variables with different units, it is needed to bring all microcirculatory features to the same magnitude. Therefore, in the current study, a demo multiple microcirculatory data set was generated by a computer algorithm based on microcirculatory characteristics of biological tissues. We aimed to transform and integrate multiple microcirculatory variables using dimensionless algorithms and to establish three-dimensional (3-D) common microcirculatory framework.

Results

Common microcirculatory framework derived from the raw microcirculatory data set. To feed the multiple microcirculatory variables embedded into the integrated 3-D common microcirculatory framework, the demo microcirculatory data set generated based on the microcirculatory function of biological tissues was imported into 3-D modules and revealed an unstandardized characteristic (Fig. 2, Supplementary Video S1). Notably, in the 3-D module without dimensionless processing, it was not allowed to generalize the integrated microcirculation in a particular condition. From the five un-normalized variables, there was an unbalanced appearance in the 3-D common framework due to the different ranges of microcirculatory oxygen and microhemodynamic parameters, which completely dominated by the larger scale (microcirculatory blood perfusion). As expected, the distribution of the data set was hard to observe considering the oscillated characteristics of microcirculatory parameters. Therefore, to integrate and visualize the global property of microcirculatory function, we next sought to compare four dimensionless methods, including Z-Score normalization, Min-max normalization, L2 normalization, and median scaling, to fit the multiple microcirculatory permutations in the established common microcirculatory framework.

Dimensionless processing in the architecture of the common microcirculatory framework. After generating the original common microcirculatory framework, subsequently, we selected four dimensionless methods that are commonly used in computational and mathematical researches to integrate the multiple microcirculatory data set and to improve the 3-D common microcirculatory framework. The transformed dimensionless microcirculatory variables were imported into the common microcirculatory framework. After dimensionless processing by Z-score normalization, there were both positive and negative values in the common framework (range from − 2 to 2), which led to difficultly couple with dynamically changed microhemodynamic and microcirculatory oxygen data set (Fig. 3, Supplementary Video S2). By contrast, all the calculated values remained positive with dimensionless

processing of Min-max normalization (Fig. 4, Supplementary Video S3), L2 normalization (Fig. 5, Supplementary Video S4), and median scaling (Fig. 6, Supplementary Video S5).

Moreover, the performance in setting a fixed range of mixed microcirculatory variables embedding in the common framework was evaluated subsequently among the four dimensionless methods. The Y axis of common microcirculatory frameworks (Fig. 3–6) and scatter plots (Fig. 7) displaying all ranges of microcirculatory variables. The ranges of the Z-score and median scaling normalized data set were [-2.50, 3.37], and [0.44, 2.12] respectively, which revealed an unfixed range. On the contrary, the entire ranges of microcirculatory features transformed by Min-max normalization and L2 normalization were mapped within the specific range [0, 1]. Therefore, Min-max normalization exhibited better performance in the processing of multiple microcirculatory variables due to both the positive values and fixed intervals.

Performance in maintaining the characteristics of multiple microcirculatory data set. To maintain the characteristics of multiple microcirculatory data set, scatter diagrams were plotted to evaluate the adaptivity of the four dimensionless methods in the processing of multiple microcirculatory variables (Fig. 7). Using microcirculatory oxygen (SO_2, rHb, PO_2) and microhemodynamic (blood perfusion and velocity) data set as input into separated dimensionless classifiers, we observed that the Z-score normalization and Min-max normalization illustrated a superior performance in reducing the distributional deformation of the original multiple microcirculatory data set. However, owing to the mathematic algorithm, dimensionless processing with L2 normalization and median scaling led to partial covering of the original characteristics. Consequently, the continuum property of microcirculatory blood perfusion and microcirculatory oxygen distribution had been better reserved after transforming by Z-score normalization and Min-max normalization comparing with L2 normalization and median scaling, which indicated a better adaptivity in the establishment of the common microcirculatory framework.

Convergency and dispersion of four dimensionless methods on multiple microcirculatory data set. The two different but connected issues with the common microcirculatory framework are convergency and dispersion. To further assess the convergency and dispersion performance of the four dimensionless methods, data set with dimensionless processing were compared in boxplots (Fig. 8A). According to the mathematical principle of interquartile range, Z-score normalization revealed a longer box indicating the dispersed microcirculatory variables although the data set had been dimensionless. While boxes of L2 normalization and median scaling limited the sensitivity of the spread of multiple microcirculatory data set and hence none of these dimensionless is desirable. Moreover, it was noted that after being dimensionless by Z-score normalization, L2 normalization, and median scaling, the microcirculatory oxygen and microhemodynamic data set were relatively influenced by the convergency and dispersion and were, therefore, less reliable. Taken together, compared to the other three dimensionless methods, the Min-max normalization was proper for the integration and visualization of multiple microcirculatory variables in common microcirculatory framework.

Furthermore, the score plots were judged on four aspects, namely positive transformed values, fixed intervals, convergence and dispersion, and identity microcirculatory property. According to the score plots

for microcirculatory oxygen (Fig. 8B) and microhemodynamics (Fig. 8C), Min-max normalization obtained better results (8 points in microcirculatory oxygen and microhemodynamic frameworks) than the other three dimensionless methods. Collectively, Min-max normalization performed better in both convergency, dispersion, and compatibility in microcirculatory data set integration and visualization, which indicated the feasibility of implementing a reliable multi-parametric common microcirculatory framework.

Discussion

Microcirculation refers to the terminal microvasculature of organs and tissues, which includes arterioles, capillaries, venules as well as micro-lymphatic vessels bridging larger and smaller scale physiological and pathological phenotypes. The microcirculation dynamically adjusts oxygen-containing blood perfusion and distribution according to the metabolic demands [16]. Global challenges to monitoring microcirculatory function are viewing the multiple parameters combinedly [17,18], rather than isolated assessment. In the current study, the common microcirculatory framework was established by computer algorithms and integration of multiple microcirculatory variables. Moreover, the multiple functional microcirculatory oxygen and microhemodynamic variables were integrated into 3-D common microcirculatory framework by Min-max dimensionless processing.

Computational and mathematical approaches have been used to analyze the functioning of the microcirculation and to establish (semi-) quantitative relationship between microvascular processes and phenomena occurring on health and diseases [19,20], leading to insights which could not be obtained solely by reductionist biological and molecular laboratory experiments. In these approaches, dimensional analysis is a method for reducing the complexity of experimental variables by using a sort of compacting algorithm [21,22]. Due to the integrity and heterogeneity of the microcirculation function of tissues, it is therefore important to develop the interpretation and analysis algorithms to extract the characteristics of the microcirculation function, integrating with the whole microcirculation function. In our case, the comparability of the raw and unstandardized integrated microcirculatory module was poor due to dimensional differences among multiple parameters of microcirculation function.

It was Secomb TW [23] that described the theoretical models of microcirculation into phenomenological, qualitative, quantitative, and predictive. To understand the complex microcirculatory system globally, our group propose to establish the common microcirculatory framework, which have been an accepted and valued aspect of researches in the field of microcirculation. Considering the characteristics of multiple microcirculatory variables, we focused on the most typical numeric variable transformation widely used. Min-max normalization can specifically fit the data set with a pre-defined boundary [24,25]. Moreover, with Min-max normalization, microcirculatory values are converted to the values within 0 to 1, which is highly dependent on the maximum and minimum microcirculatory functional values and therefore particularly sensitive to outliers. This is the reason that we performed a filter by automated pre-process outlier module to fix the interval, through which the demo microcirculatory data set are less likely to flock in a specific subrange and work better in the 3-D coordinate rather than masking the microcirculatory properties.

One advantage of Z-score normalization appears to be the ability to minimize the distortion introduced to the microcirculatory data set. Although Z-score normalization is suitable for normal distribution data [26], however, an apparent drawback of Z-score normalization is that the return microcirculatory value after processing can be negative. In this situation, we have to extend the X axis and Y axis to deal with negative coordinates, which is not conducive to the integration of dynamically changed microhemodynamic and microcirculatory oxygen data set [27–29] in the common microcirculatory framework.

Encoding microcirculatory data set by L2 normalization and median scaling eliminates or partially dilutes the original characteristics due to the mathematic algorithm. The L2 normalization assumes that the values of a data set are separated by a constant. Median scaling simply moves the plot up so that the median difference is 0. Hence, both dimensionless methods are not correct the non-linear bias of microcirculatory variables. Moreover, blood perfusion in the microcirculation differs substantially from blood flow in large vessels. In the microcirculation, inertial effects, as well as pulsatility (so-called vasomotion), are partially neglected. L2 normalization is prone to losing information about the scale of inputs of multiple microcirculatory variables, which hamper separating datapoint for the entire microcirculatory data set. Compared with Z-score normalization, L2 normalization, and median scaling, the continuum property of microhemodynamic and microcirculatory oxygen distribution has been better reserved by Min-max normalization.

Additionally, the accuracy and reliability of the microcirculatory functional values are two important determinants of the common microcirculatory framework. Hence, it is necessary to pre-process outliers for the input data set [30]. Comparing various outlier processing algorithms (missing values, mean correction, etc.) [31,32], in our case, the pre-process of outliers was managed through the script embedding boxplot and least common multiple algorithm, values beyond the boundary were regarded as outliers and automatically adjusted to the nearest boundary value to maintain the identity characteristics of microcirculatory functional data set.

So far, we have revealed dimensional homogeneity using Min-max normalization for converting a homogeneous physiological relation to a dimensionless type. Although the method is straightforward mathematically, there are certain limitations that need to be discussed. First, the selection of important microcirculatory variables requires judgment. Not all microcirculatory parameters, take the rheological properties (viscosity and hematocrit values) for instance, are available and embedded in our common microcirculatory framework. Researchers should decide whether viscosity can be neglected in the specific application. Furthermore, once the dimensionless analysis is performed, the similarity between the models and algorithms are needed sufficient testing.

In conclusion, important microhemodynamic and microcirculatory oxygen variables are embedded in the proposed function through the scaling law of Min-max normalization, which converts the microcirculatory data set from multiple parameters to an integrated 3-D common microcirculatory framework. Therefore, our current study provides methodological support and a novel paradigm for the analysis of integrated

microcirculation function of organs and tissues, and pave the way for further exploring the associations between microcirculation and diseases.

Methods

Construction and description of the common microcirculatory framework. The common microcirculatory framework was generally constructed by multimodal laser Doppler-equipped devices and computer algorithm-based modules (Fig. 1). Oxygen to See (O2C, LEA Medizintechnik GmbH, Giessen, Germany), micro fiber-optic oxygen transmitter (Microx TX3, PreSens, Precision Sensing GmbH, Regensburg, Germany), and a dual-channel laser Doppler monitoring instrument (VMS-LDF2, Moor Instruments, Ltd., Axminster, UK) were employed to generate microcirculatory oxygen and microhemodynamic parameters, including hemoglobin oxygen saturation (SO_2), the relative amount of hemoglobin (rHb), partial oxygen pressure (PO_2), microvascular blood perfusion, and blood flow velocity.

Demo microcirculatory permutations were generated by a computer algorithm based on the technical guideline of equipment and the characteristics of microcirculatory oxygen and microhemodynamics of biological tissues. The ranges and dimensions (units) of microcirculatory SO_2, rHb, PO_2, blood perfusion, and blood flow velocity were listed in Supplementary Table S1. Subsequently, Python (version 3.7.4, https://www.python.org) and Apache ECharts (Version 4.2.0-RC.2, https://echarts.apache) were used to establish the 3-D common microcirculatory framework, in which the time course, multiple variables, and demo microcirculatory values were defined as X, Y, and Z axes, respectively.

Data preprocessing of common microcirculatory framework. Outliers are extreme values that deviate from the majority of observations on the microcirculatory data set. In our preprocessing module, outliers in the common microcirculatory framework were detected by the boxplot algorithm. We defined Q_1 as the 25th percentile largest value and Q_3 as the 75th percentile largest value, so that the difference between Q_3 and Q_1 is the interquartile range (IQR). Values of microcirculatory variables over the range from (Q_1-1.5×IQR) to (Q_3+1.5×IQR) were considered as outliers and were adjusted to the nearest boundary value automatically. With the outliers preprocessing procedure, all microcirculatory data set were embedded into the common microcirculatory framework. Besides, the least common multiple algorithm was used to ensure the consistency of data size exhibiting in the common microcirculatory framework.

Comparison of dimensionless methods on the establishment of the common microcirculatory framework. Normalization is one of the most important steps in multiple microcirculatory variables analysis. For our common microcirculatory framework, the data set of five microcirculatory variables differ in dimension and range. To integrate these microcirculatory variables and visualize the global functional status of microcirculation, four common dimensionless methods, including Z-score normalization, Min-max normalization, L2 normalization, and median scaling, were selected to make the microcirculatory data set dimensionless.

Z-score normalization is a strategy of normalizing data set that avoids outlier issue. After Z-score processing, the original microcirculatory data set was converted to be squished on the same scale for the features. The absolute value of z represents the distance between that raw microcirculatory data set and the mean in units of the standard deviation. The data set processing equation of Z-score normalization is as follows:

$$x' = \frac{x-\bar{x}}{\sigma} \quad (1)$$

where x is the original microcirculatory variable. $\bar{x}$ represents the mean value of the microcirculatory feature. σ is the standard deviation.

Min-max normalization, known as deviation normalization, processes data set based on extreme values and classify the processed data into the range of [0, 1]. The minimum value of the microcirculatory data set was transformed into a 0, and the maximum value was transformed into a 1. Subsequently, every value was transformed into a decimal between 0 and 1. The data set processing equation of Min-max normalization is as follows:

$$x' = \frac{x-min}{max-min} \quad (2)$$

where min and max are the minimum and maximum values of the microcirculatory data set, respectively.

L2 normalization is an alternative method widely used in dimensionless scaling for multiple data set [33], which measures the length or size of vectors and scales the components of feature vector. Each microcirculatory component was divided by the Euclidean length of the vector. The data set processing equation of L2 normalization is:

$$x_i' = \frac{x_i}{norm(x)} \quad (3)$$

Where $norm(x)$ is:

$$norm(x) = \sqrt{{x_1}^2 + {x_2}^2 + \cdots + {x_n}^2} \quad (4)$$

Median scaling represents the nonparametric method of standardization (centering and scaling) [34]. All microcirculatory data set were divided by the median. The data set processing equation of median scaling is:

$$x' = \frac{x}{Me} \quad (5)$$

Where Me is the median of the microcirculatory data set.

Visualization and video recording of dynamic common microcirculatory framework. A video recording software, ScreenToGif (version 2.19.3, URL: https://www.screentogif.com/), was employed to record the dynamic common microcirculatory framework processed with Z-Score normalization, Min-Max normalization, L2 normalization, and median scaling, respectively. Each video was saved in the format of MP4 with duration of approximately 1 min. The bitrate of the video was approximately 1000 Kbps with 1518 × 816 in resolution ratio.

Scoring of the performance of dimensionless methods. To qualify the performance of four dimensionless methods (Z-score normalization, Min-max normalization, L2 normalization, and median scaling) in the pre-processing of multiple microcirculatory variables and the establishment of the common microcirculatory framework, a scoring system was constructed. In the scoring system, the final score is a weighted composite of the four scores from each independent performance category. The four categories are positive values, fixed intervals, convergence/dispersion, and the extent of maintaining identity property of microcirculatory data set, reflecting the integration efficiency, compatibility, and adaptivity of four dimensionless methods on the establishment and visualization of the common microcirculatory framework. Each category was scored individually (2 points for each category) and summed to calculate the final score. Moreover, considering the heterogeneity of microcirculatory variables, dimensionless performance in microcirculatory oxygen and microhemodynamics were scored separately.

Declarations

Data availability

Requests for access to data should be addressed to the corresponding author.

Acknowledgments

We thank Xi'nan Duan for the discussion about the computational algorithm.

Author contributions

M. L. and Y. L. designed the study and drafted the manuscript. X. Z. and X. L. collected the data. Y. L., B. W., B. L., Q. W., and M. L. analyzed the data. M. L., J. Z., H. Z., and R. X. critically revised manuscript and final approval.

Competing interests

The authors declare no competing interests.

Additional information

Supplementary Information The online version contains supplementary material available at https://doi.org/10.6084/m9.figshare.13311512.

References

1 Saldivar, E., Cabrales, P., Tsai, A. G. & Intaglietta, M. Microcirculatory changes during chronic adaptation to hypoxia. *American journal of physiology. Heart and circulatory physiology* **285,** H2064-H2071, doi:10.1152/ajpheart.00349.2003 (2003).

2 Trzeciak, S. & Rivers, E. P. Clinical manifestations of disordered microcirculatory perfusion in severe sepsis. *Critical care* **9,** S20-S26, doi:10.1186/cc3744 (2005).

3 Kord Valeshabad, A. *et al.* Conjunctival microvascular haemodynamics in sickle cell retinopathy. *Acta Ophthalmol* **93,** e275-e280, doi:10.1111/aos.12593 (2015).

4 Vandenbulcke, L. *et al.* Microvascular reactivity monitored with near-infrared spectroscopy is impaired after induction of anaesthesia in cardiac surgery patients: An observational study. *European journal of anaesthesiology* **34,** 688-694, doi:10.1097/EJA.0000000000000684 (2017).

5 De Backer, D. *et al.* Monitoring the microcirculation in the critically ill patient: current methods and future approaches. *Intensive Care Med.* **36,** 1813-1825, doi:10.1007/s00134-010-2005-3 (2010).

6 Chipperfield, A. J., Thanaj, M., Scorletti, E., Byrne, C. D. & Clough, G. F. Multi-domain analysis of microvascular flow motion dynamics in NAFLD. *Microcirculation* **26,** e12538, doi:10.1111/micc.12538 (2019).

7 Frisbee, J. C., Lewis, M. T. & Wiseman, R. W. Skeletal muscle performance in metabolic disease: Microvascular or mitochondrial limitation or both? *Microcirculation* **26,** e12517, doi:10.1111/micc.12517 (2019).

8 Adolphs, J. *et al.* Effects of thoracic epidural anaesthesia on intestinal microvascular perfusion in a rodent model of normotensive endotoxaemia. *Intensive care medicine* **30,** 2094-2101, doi:10.1007/s00134-004-2426-y (2004).

9 Potus, F. *et al.* Impaired angiogenesis and peripheral muscle microcirculation loss contribute to exercise intolerance in pulmonary arterial hypertension. *American journal of respiratory and critical care medicine* **190,** 318-328, doi:10.1164/rccm.201402-0383OC (2014).

10 Roustit, M. & Cracowski, J. L. Assessment of endothelial and neurovascular function in human skin microcirculation. *Trends in pharmacological sciences* **34,** 373-384, doi:10.1016/j.tips.2013.05.007 (2013).

11 Corliss, B. A., Mathews, C., Doty, R., Rohde, G. & Peirce, S. M. Methods to label, image, and analyze the complex structural architectures of microvascular networks. *Microcirculation* **26,** e12520, doi:10.1111/micc.12520 (2019).

12 Goldman, D., Farid, Z. & Jackson, D. N. A streak length-based method for quantifying red blood cell flow in skeletal muscle arteriolar networks. *Microcirculation* **26,** e12532, doi:10.1111/micc.12532 (2019).

13 Yang, C. S. *et al.* Rapid long-wave infrared laser-induced breakdown spectroscopy measurements using a mercury-cadmium-telluride linear array detection system. *Applied optics* **54,** 9695-9702, doi:10.1364/AO.54.009695 (2015).

14 Colantuoni, C., Henry, G., Zeger, S. & Pevsner, J. SNOMAD (Standardization and NOrmalization of MicroArray Data): web-accessible gene expression data analysis. *Bioinformatics* **18,** 1540-1541, doi:10.1093/bioinformatics/18.11.1540 (2002).

15 Cao, X. H., Stojkovic, I. & Obradovic, Z. A robust data scaling algorithm to improve classification accuracies in biomedical data. *BMC bioinformatics* **17,** 359, doi:10.1186/s12859-016-1236-x (2016).

16 Gutterman, D. D. *et al.* The Human Microcirculation: Regulation of Flow and Beyond. *Circ. Res.* **118,** 157-172, doi:10.1161/CIRCRESAHA.115.305364 (2016).

17 Scheeren, T. W. Monitoring the microcirculation in the critically ill patient: reflectance spectroscopy. *Intensive Care Med.* **37,** 1045-1046, doi:10.1007/s00134-011-2197-1 (2011).

18 Ansari, M. Z., Kang, E. J., Manole, M. D., Dreier, J. P. & Humeau-Heurtier, A. Monitoring microvascular perfusion variations with laser speckle contrast imaging using a view-based temporal template method. *Microvascular research* **111,** 49-59, doi:10.1016/j.mvr.2016.12.004 (2017).

19 Possenti, L. *et al.* A computational model for microcirculation including Fahraeus-Lindqvist effect, plasma skimming and fluid exchange with the tissue interstitium. *Int J Numer Method Biomed Eng* **35,** e3165, doi:10.1002/cnm.3165 (2019).

20 Piergiovanni, M. *et al.* Microcirculation in the murine liver: a computational fluid dynamic model based on 3D reconstruction from in vivo microscopy. *Journal of biomechanics* **63,** 125-134, doi:10.1016/j.jbiomech.2017.08.011 (2017).

21 Fries, N. & Dreyer, M. Dimensionless scaling methods for capillary rise. *J Colloid Interface Sci* **338,** 514-518, doi:10.1016/j.jcis.2009.06.036 (2009).

22 Allen, T. A., Schreiber, A. M., Hall, N. T. & Hallquist, M. N. From Description to Explanation: Integrating Across Multiple Levels of Analysis to Inform Neuroscientific Accounts of Dimensional Personality Pathology. *J Pers Disord* **34,** 650-676, doi:10.1521/pedi.2020.34.5.650 (2020).

23 Secomb, T. W., Beard, D. A., Frisbee, J. C., Smith, N. P. & Pries, A. R. The role of theoretical modeling in microcirculation research. *Microcirculation* **15,** 693-698, doi:10.1080/10739680802349734 (2008).

24 Raghavan, K., Garg, S., Jagannathan, S. & Samaranayake, V. A. Distributed Min-Max Learning Scheme for Neural Networks With Applications to High-Dimensional Classification. *IEEE transactions on neural networks and learning systems* **PP,** 1-11, doi:10.1109/TNNLS.2020.3017434 (2020).

25 Liu, Y., Buck, J. R. & Ikonomidou, V. N. Generalized min-max bound-based MRI pulse sequence design framework for wide-range T1 relaxometry: A case study on the tissue specific imaging sequence. *PloS one* **12,** e0172573, doi:10.1371/journal.pone.0172573 (2017).

26 Dallaire, F. *et al.* Pediatric Reference Values and Z Score Equations for Left Ventricular Systolic Strain Measured by Two-Dimensional Speckle-Tracking Echocardiography. *J. Am. Soc. Echocardiogr.* **29,** 786-793.e788, doi:10.1016/j.echo.2016.03.018 (2016).

27 Liu, M. *et al.* Laser Doppler: A Tool for Measuring Pancreatic Islet Microvascular Vasomotion In Vivo. *Journal of visualized experiments : JoVE* **3,** e56028, doi:10.3791/56028 (2018).

28 Thorn, C. E., Kyte, H., Slaff, D. W. & Shore, A. C. An association between vasomotion and oxygen extraction. *American journal of physiology. Heart and circulatory physiology* **301,** H442-H449, doi:10.1152/ajpheart.01316.2010 (2011).

29 Kislukhin, V. V. Stochasticity of flow through microcirculation as a regulator of oxygen delivery. *Theoretical biology & medical modelling* **7:29,** doi:10.1186/1742-4682-7-29 (2010).

30 Yu, K., Shi, W. & Santoro, N. Designing a Streaming Algorithm for Outlier Detection in Data Mining-An Incrementa Approach. *Sensors (Basel)* **20,** 1261, doi:10.3390/s20051261 (2020).

31 Sondag, P., Zeng, L., Yu, B., Yang, H. & Novick, S. Comparisons of outlier tests for potency bioassays. *Pharm Stat* **19,** 230-242, doi:10.1002/pst.1984 (2020).

32 Xie, W., Chkrebtii, O. & Kurtek, S. Visualization and Outlier Detection for Multivariate Elastic Curve Data. *IEEE transactions on visualization and computer graphics* **26,** 3353-3364,

doi:10.1109/TVCG.2019.2921541 (2020).

33 Yu, S. *et al.* L2-norm multiple kernel learning and its application to biomedical data fusion. *BMC bioinformatics* **11,** 309, doi:10.1186/1471-2105-11-309 (2010).

34 Khan, D. Z. *et al.* Robotic Semi-Automated Transcranial Doppler Assessment of Cerebrovascular Autoregulation in Post-Concussion Syndrome: Methodological Considerations. *Neurotrauma Rep* **1,** 218-231, doi:10.1089/neur.2020.0021 (2020).

Figures

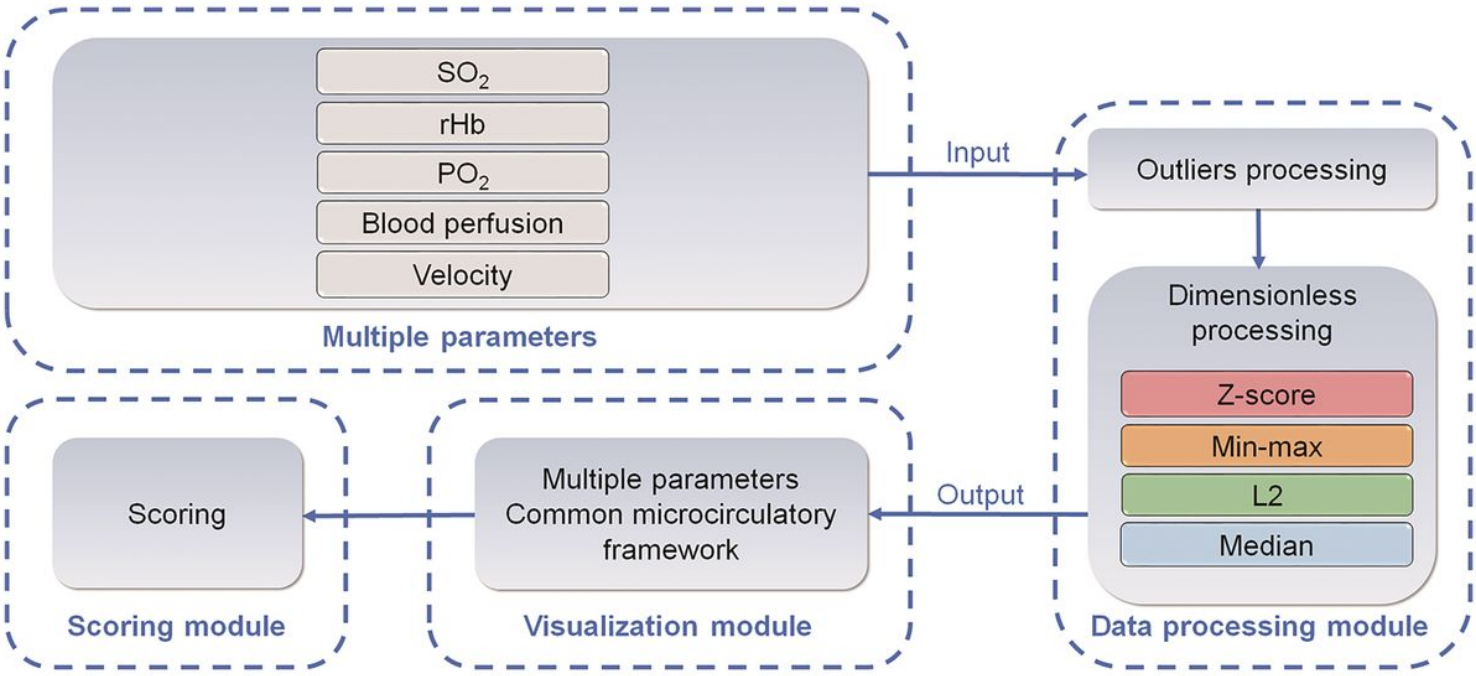

Figure 1

Schematic of the multimodal device and computer algorithm-based common microcirculatory framework and dimensionless analysis. Arrows denote the directional flow of the demo microcirculatory data set. Multiple microcirculatory parameters, including hemoglobin oxygen saturation (SO2), the relative amount of hemoglobin (rHb), partial oxygen pressure (PO2), microvascular blood perfusion, and blood flow velocity, were generated and inputted into the data processing module. After the automated adjustment of outliers, the microhemodynamic and microcirculatory oxygen data set were transformed to be dimensionless in the data processing module by Z-score normalization, Min-max normalization, L2 normalization, and median scaling, respectively. The pre-processed and dimensionless microcirculatory variables were then integrated and visualized as a three-dimensional (3-D) common microcirculatory framework. The integration efficiency, compatibility, and adaptability of four dimensionless methods on establishing the 3-D common microcirculatory framework were scored and assessed.

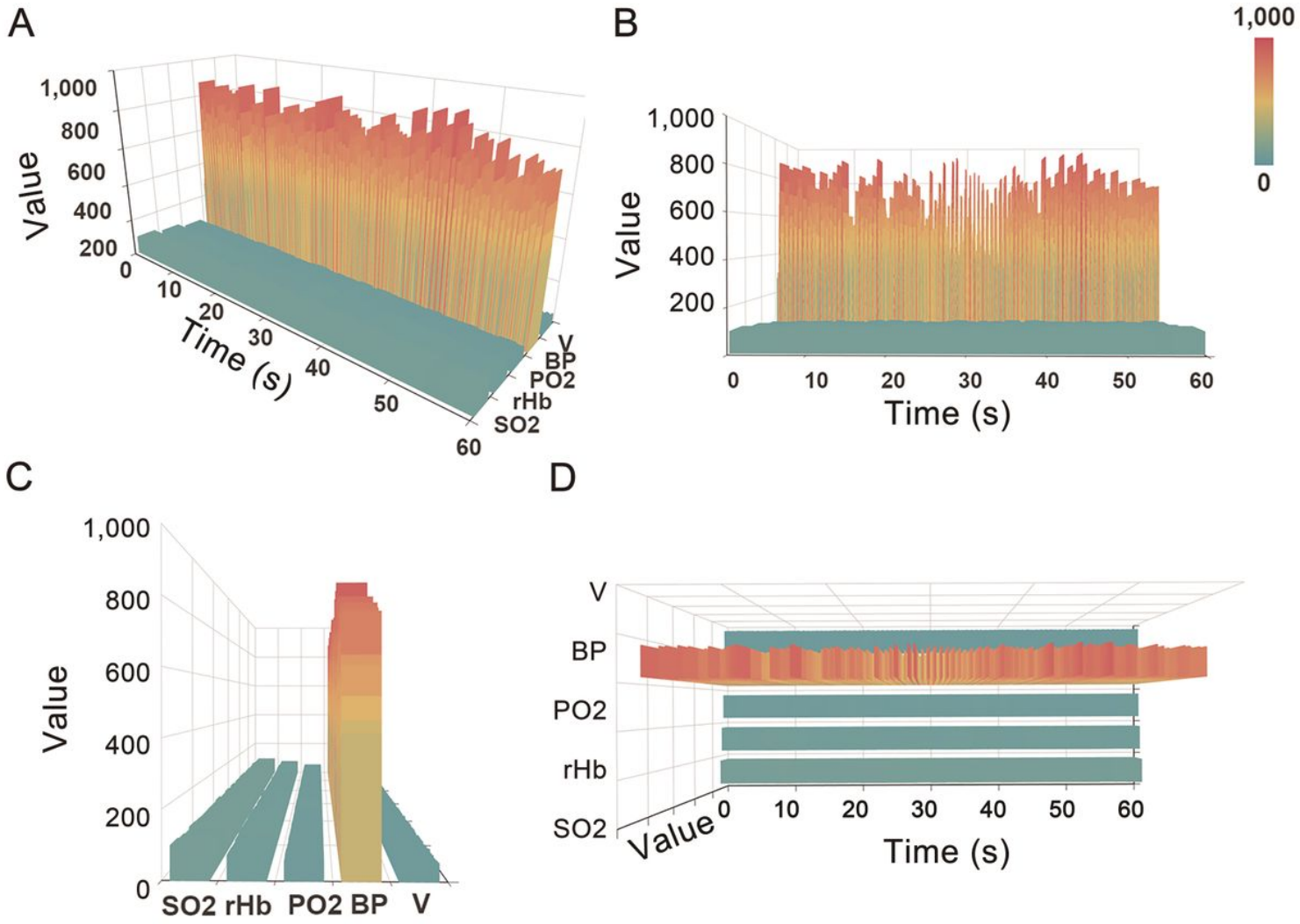

Figure 2

Unnormalized common microcirculatory framework. The 3-D common microcirculatory framework was established by Python (version 3.7.4, https://www.python.org) and Apache ECharts (released version 4.2.0-RC.2, https://echarts.apache.org), reflecting the integrated functional status of microcirculation. Multiple microcirculatory variables of the data set (including hemoglobin oxygen saturation, the relative amount of hemoglobin, partial oxygen pressure, microvascular blood perfusion, and blood flow velocity) were embedded without pre-processing and normalized. The X, Y, and Z axis represent the time course, microcirculatory variables, and normalized values, respectively. (A) The straight view of the common microcirculatory framework was rotated 45 degrees towards the left. (B) The front view. (C) The side view was rotated 90 degrees towards the left. (D) The vertical view of the common microcirculatory framework was generated 90 degrees toward down. Color bars in the 3-D common microcirculatory framework represent the real values of the data set. SO2, hemoglobin oxygen saturation. rHb, the relative amount of hemoglobin. PO2, partial oxygen pressure. (Supplementary Video S1, doi: https://doi.org/10.6084/m9.figshare.13311512).

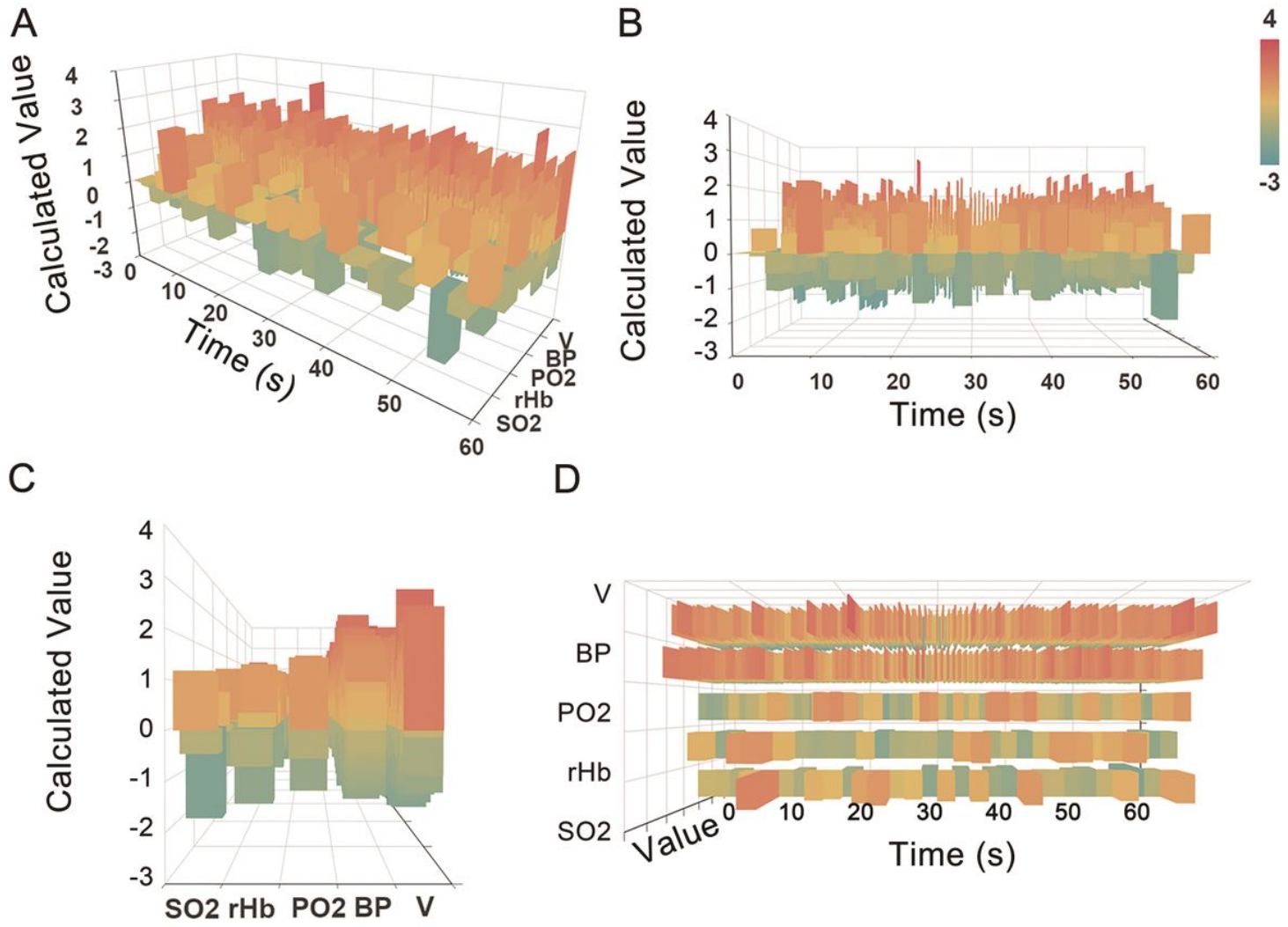

Figure 3

Z-score normalized common microcirculatory framework. Pre-processed by Z-score normalization, microhemodynamic, and microcirculatory oxygen profiles were integrated into the 3-D common microcirculatory framework. (A-D) Views of Z-score normalized common microcirculatory framework generating by rotation as mentioned above. (A) Straight view; (B) Front view; (C) Side view; (D) Vertical view. Color bars in the 3-D common microcirculatory framework represent the normalized values of the data set. SO2, hemoglobin oxygen saturation. rHb, the relative amount of hemoglobin. PO2, partial oxygen pressure. (Supplementary Video S2, doi: https://doi.org/10.6084/m9.figshare.13311512).

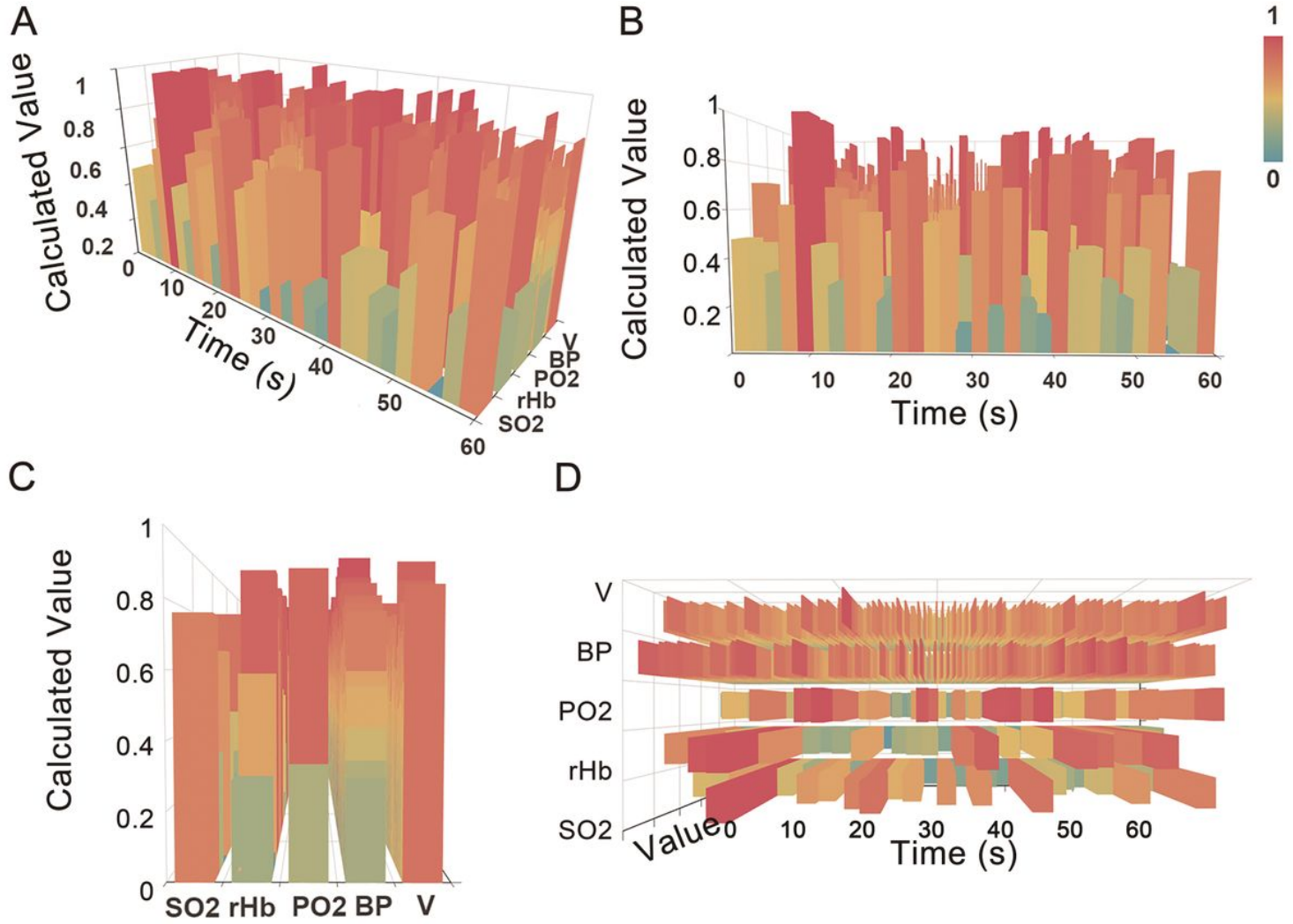

Figure 4

Min-max normalized common microcirculatory framework. Under the principle of Min-max normalization, the minimum value of the microcirculatory data set was transformed into a 0, and the maximum value was transformed into a 1. The microcirculatory data set was transformed into the range of [0, 1], and was integrated into the 3-D common microcirculatory framework. (A-D) Views of Min-max normalized common microcirculatory framework generating by rotation. (A) Straight view, (B) Front view, (C) Side view, and (D) Vertical view of the 3-D common microcirculatory framework. Color bars in the 3-D common microcirculatory framework represent the normalized values of the data set. SO2, hemoglobin oxygen saturation. rHb, the relative amount of hemoglobin. PO2, partial oxygen pressure. (Supplementary Video S3, doi: https://doi.org/10.6084/m9.figshare.13311512).

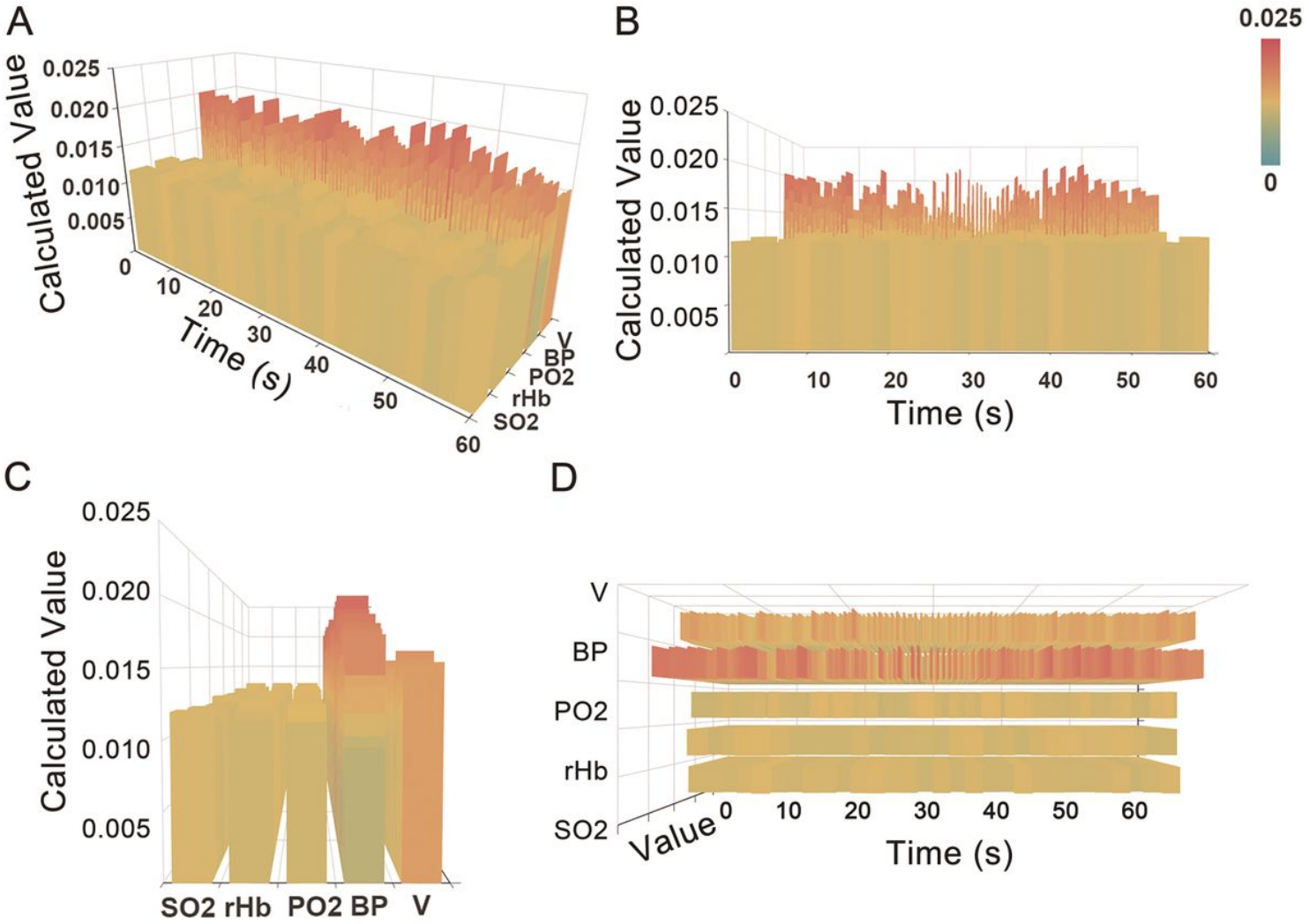

Figure 5

L2 normalized common microcirculatory framework. L2 normalization strategy has been applied to fit 3-D common microcirculatory framework. (A-D) Views of L2 normalized common microcirculatory framework generating by rotation (A) Straight view; (B) Front view; (C) Side view; (D) Vertical view. Color bars in the 3-D common microcirculatory framework represent the normalized values of the data set. SO2, hemoglobin oxygen saturation. rHb, the relative amount of hemoglobin. PO2, partial oxygen pressure. (Supplementary Video S4, doi: https://doi.org/10.6084/m9.figshare.13311512).

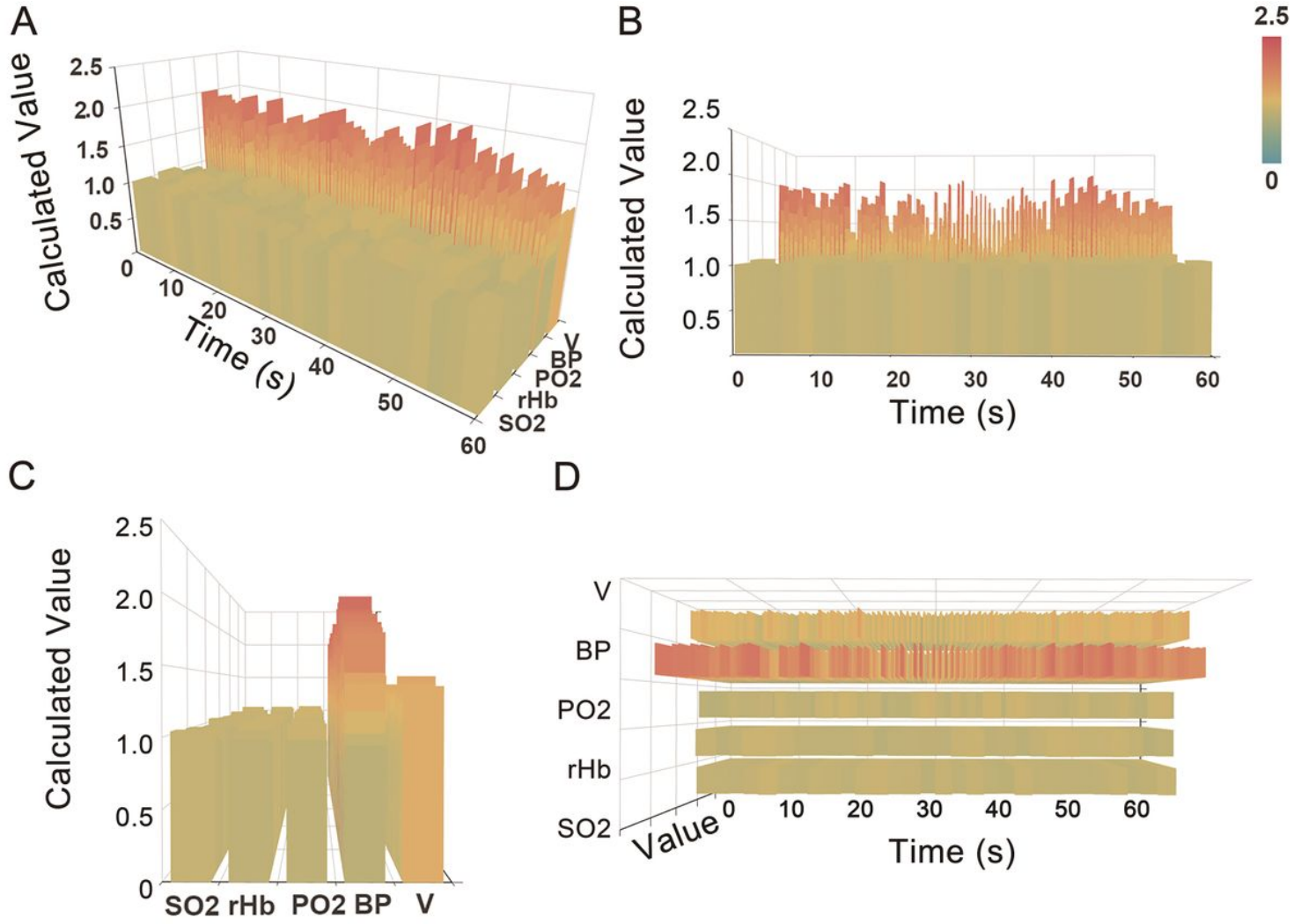

Figure 6

Median scaling normalized common microcirculatory framework. The multiple microcirculatory variables were normalized by median scaling. Values of microcirculatory oxygen and microhemodynamics were divided by the corresponding median. After scaling, the microcirculatory data set was integrated into the 3-D common microcirculatory framework. (A-D) Global views of 3-D common microcirculatory framework normalized by median scaling method. (A) Straight view; (B) Front view; (C) Side view; (D) Vertical view. Color bars in the 3-D common microcirculatory framework represent the normalized values of the data set. SO2, hemoglobin oxygen saturation. rHb, the relative amount of hemoglobin. PO2, partial oxygen pressure. (Supplementary Video S5, doi: https://doi.org/10.6084/m9.figshare.13311512).

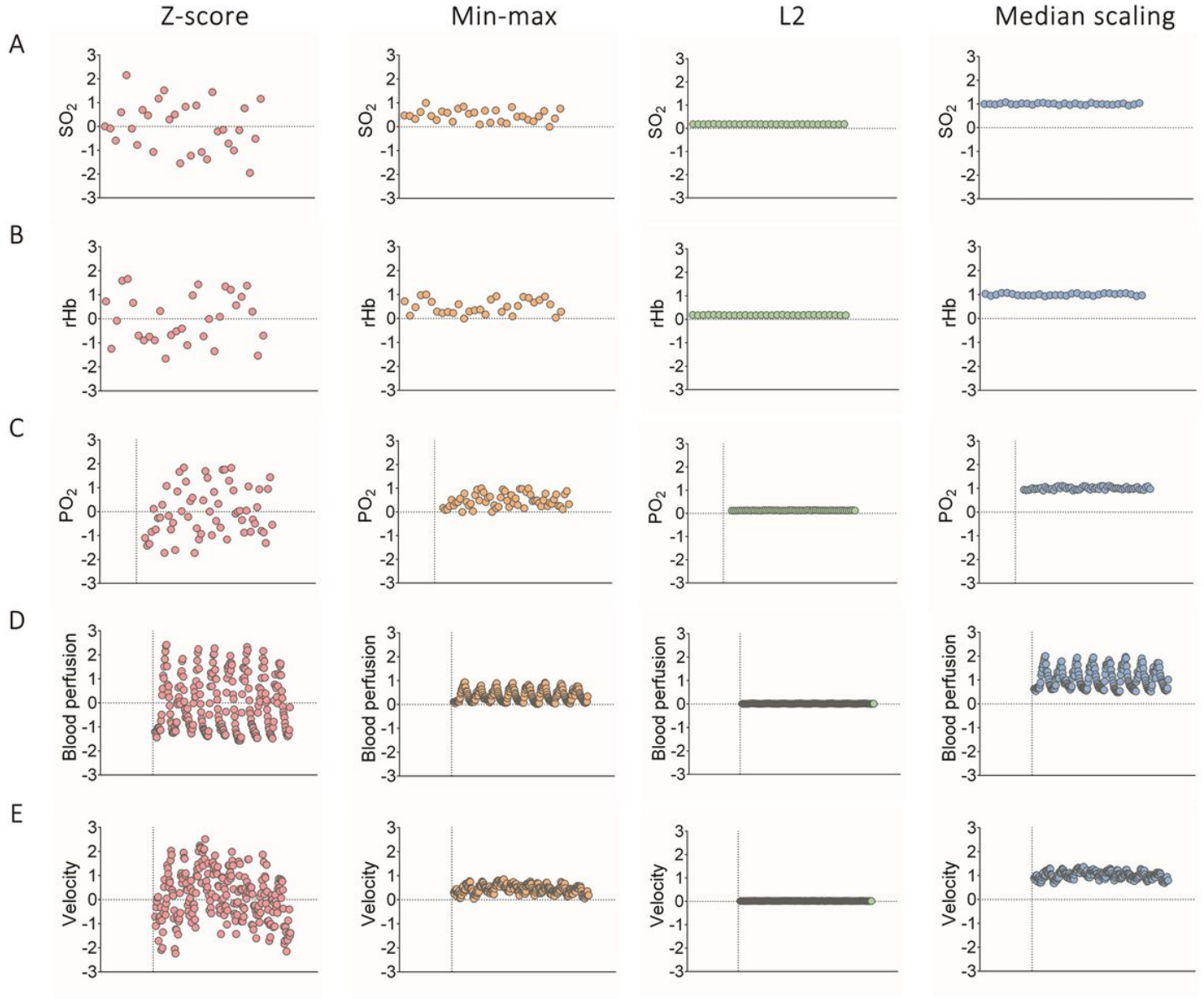

Figure 7

Performance of four dimensionless methods in maintaining identity property of microcirculatory data set. After transforming by the four dimensionless methods (Z-score normalization, Min-max normalization, L2 normalization, and median scaling), microcirculatory oxygen and microhemodynamic values (including SO2, rHb, PO2, blood perfusion, and velocity) were illustrated in the scatter plots, which represents the property of multiple microcirculatory parameters. (A-E) Distribution of the multiple microcirculatory variables with dimensionless processing. (A) SO2, (B) rHb, (C) PO2, (D) Blood perfusion, and (E) Velocity. The dotted line represents zero value. Red dot, dimensionless microcirculatory variable processed by Z-score normalization. Yellow dot, dimensionless microcirculatory variable transformed by Min-max normalization. Green dot, normalized microcirculatory value processed by L2 normalization. The blue dot represents the median scaling processed microcirculatory value. SO2, hemoglobin oxygen saturation. rHb, the relative amount of hemoglobin. PO2, partial oxygen pressure.

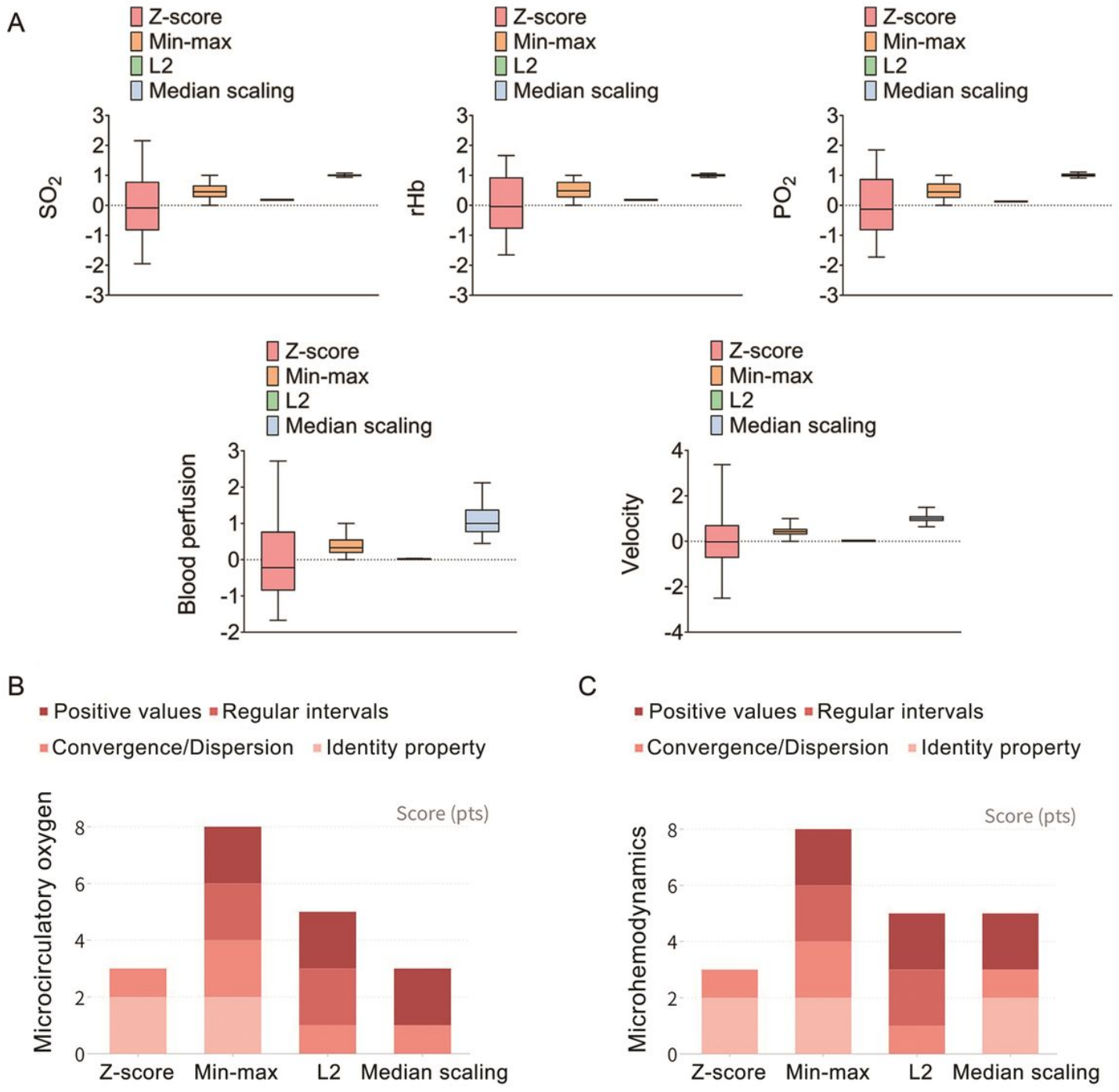

Figure 8

Performance of four dimensionless methods in microcirculatory data set processing. The integration efficiency, compatibility, and adaptivity of the four dimensionless methods (Z-score normalization, Min-max normalization, L2 normalization, and median scaling) in the pre-processing of multiple microcirculatory variables and in the establishment of common microcirculatory framework were compared and scored. (A) The capabilities of convergency and dispersion were illustrated as boxplots. The boxplot covered the values from the 25th percentile largest value to the 75th percentile largest value with the median values marked as black lines in each of the boxes. The whiskers indicated the minimum

and maximum of each normalized microcirculatory variables. The dotted lines represent zero values. Red represents dimensionless microcirculatory variable processed by Z-score normalization. Yellow represents Min-max normalization. Green represents L2 normalization, and blue represents median scaling, respectively. (B-C) Scores of four dimensionless methods. The scoring system was introduced across four dimensionless methods to evaluate integration efficiency, compatibility, and adaptivity. There were four independent aspects in the scoring system (2 points for each aspect), namely positive values, regular intervals, convergence/dispersion, and the extent of maintaining identity property of microcirculatory data set. The sum of the scores for each dimensionless method is tallied and compared. SO2, hemoglobin oxygen saturation. rHb, the relative amount of hemoglobin. PO2, partial oxygen pressure.

Supplementary Files

This is a list of supplementary files associated with this preprint. Click to download.

- SupplementaryInfomation.pdf